Investigation of the Characteristics of Nanofluids Flow and Heat Transfer in a Pipe using a Single Phase Model

Goutam Saha[a,b] and Manosh C. Paul[a,*]

[a]Systems, Power and Energy Research Division, School of Engineering, University of Glasgow, Glasgow G12 8QQ, UK

[b]Department of Mathematics, University of Dhaka, Dhaka-1000, Bangladesh

**Corresponding author.* Tel.: +44(0)141 330 8466;Manosh.Paul@glasgow.ac.uk

Abstract

Single phase model has been used to investigate the flow characteristics of Al_2O_3–water and TiO_2–water nanofluids in a horizontal pipe under constant heat flux boundary condition. SST $\kappa - \omega$ model has been applied to simulate the flow and thermal fields for a number of physical, thermal and nanofluid conditions. Results generally reveal that the enhancement of heat transfer and entropy generation is dependent on the concentrations, size of nanoparticles and flow Reynolds number. However, the heat transfer rate is predicted to be little bit higher for the Al_2O_3–water nanofluid than that of the TiO_2–water nanofluid. It is also found that there exists no optimal Reynolds number for which the total entropy generation could be optimised. Some new correlations have been proposed and used them to calculate the average Nusselt number using single phase model.

Keywords: Nanofluid; heat transfer; entropy generation; single phase model; shear stress ratio.

1. Introduction

Reynolds [1] found the transition flow behaviour to change unpredictably between the laminar and turbulent flow. It is observed in this research that the laminar flow can be sustained at high Reynolds numbers if different types of disturbances in the flow are eluded (Cengel[2]). Later on, Ekman [3] and Pfenniger [4] performed experimental investigations and stated that the laminar flow could have been maintained up to a Reynolds number of $40{,}000$ and $100{,}000$ respectively by reducing the flow disturbances. Cengel [2] also suggested, that it was better to have some specific values of Reynolds number for laminar, transitional and turbulent flows in a smooth pipe. But this was tricky since flow disturbances were generated by various mechanisms such as surface roughness, noise, and vibrations. In most cases, the flow in a smooth pipe is said to be laminar when $Re < 2300$, fully turbulent when $Re > 10{,}000$ and transitional when $2300 \leq Re \leq 10{,}000$. Cengel [2] however stated that even though transitional flow exists for $2300 \leq Re \leq 10{,}000$, a fully turbulent condition in many practical applications can be achieved when $Re > 4000$.

We know that internal flow behaves like a laminar flow when flow pattern of fluids forms a parallel layer inside the domain with no disturbance between the layers. But, imposing external disturbance can make the flow unstable sometimes. This can be seen from the flow fields where small fluctuation occurs in the parallel layer. Such behaviour is known as transitional behaviour and we simply say that transition flow is a state between the laminar and turbulent flow. It is important to note that the flow in a smooth pipe is said to be transitional when $2300 \leq Re \leq 10{,}000$. Very few researches have been done on pipe under transition flow region and most of them were experimental and details are discussed in the following section:

Tang *et al.* [5] experimentally investigated the hydrodynamic behaviour of Al_2O_3–water nanofluid flowing through a horizontal tube. Their results indicated that transition flow had been monitored at $Re{\sim}1500$ comparing with $Re{\sim}2300$ given in Cengel [2] for the transition regime. It suggested, the transition regime could start from $Re{\sim}1500$ although many researchers monitored it to be $2000 < Re < 4000$. However, few works have been done on horizontal tube with twisted tape or wire coil inserts in order to see the effect on the heat transfer performance under transition flow condition. Sharma *et al.* [6] and Chandrasekar *et al.* [7] observed the heat transfer behaviour experimentally using Al_2O_3–water nanofluid flowing through a circular tube with twisted tape or wire coil inserted under the transitional flow regime. The maximum heat transfer enhancement of 20% and 23.07% had been achieved for $\chi = 0.1\%$ at $Re = 5000$ and $Re = 9000$ respectively. A similar experimental investigation was done by Naik *et al.* [8] for water–propylene glycol based CuO nanofluid and the maximum enhancement of 76.06% had been attained at $Re = 10000$ and for $\chi = 0.5\%$. Analysing their findings, it is concluded that maximum enhancement of heat transfer can be observed for the high Reynolds number. Meyer *et al.* [9], first time in the recent years, has experimentally investigated

the heat transfer behaviour influenced by multi-walled carbon nanotubes inside the smooth horizontal tube under transitional flow regime. In their investigation, transition flow behaviour is observed in between $2900 \leq Re \leq 3600$. They have mentioned, the heat transfer rate decreases while using multi-walled carbon nanotubes.

Recently, effect of concentrations, size diameters and Brownian motion of nanoparticles on the convective heat transfer and entropy generation of Al_2O_3 and TiO_2–water nanofluids have been investigated by Saha and Paul [10, 11] using both single and multi-phase models. However, no research has been found to understand the heat transfer and entropy generation behaviour of Al_2O_3 and TiO_2–water nanofluids flowing through a horizontal pipe using smooth pipe wall under the transitional to turbulent flow regimes. Hence, the main objective of this research is to analyse the effects of different nanoparticles size and concentrations with the Brownian motion of nanoparticles on heat transfer under transition to turbulent flow condition. Finally, results have been presented in terms of local and average Nusselt number, average wall shear stress coefficient ratio, thermal performance factor and entropy generation.

2. Mathematical Modelling

In this research, numerical investigations have been carried out using single phase model. Here, two-dimensional axi-symmetric model of a horizontal pipe with the length L of $1.0\,m$ and internal diameter, D_h of $0.019\,m$ has been considered to analysis the heat transfer performance of Al_2O_3 and TiO_2–water nanofluids through it. The geometry is shown in Fig. 1. Also, the dimensional steady-state governing equations of fluid flow and heat transfer for the single phase modelis presented under the following assumptions:

- Fluid flow is incompressible, Newtonian and transitional,
- The Boussinesq approximation is negligible as the pipe is placed horizontally,
- Fluid phase and nanoparticle phase are in thermal equilibrium with no-slip between them,
- Nanoparticles are spherical and uniform in size and shape,
- Radiation effects and viscous dissipation are negligible.

Continuity equation:

$$\nabla.\left(\rho_m \vec{V}_m\right) = 0 \tag{1}$$

Momentum equation:

$$\nabla.\left(\rho_m \vec{V}_m \vec{V}_m\right) = -\nabla P_m + \nabla.\left[\mu_m\left(\nabla \vec{V}_m + \nabla\, \vec{V}_m^{T}\right) - \frac{2}{3}\nabla.\,\vec{V}_m\right] + \rho_m \vec{g} \tag{2}$$

Energy equation:

$$\nabla.\left(\rho_m \vec{V}_m C_p T\right) = \nabla.\left(\lambda_m \nabla T\right) \tag{3}$$

where $\vec{V}_m, \rho_m, \mu_m, \lambda_m, \vec{g}$ are the mass-average velocity, mixture density, viscosity of the mixture and mixture thermal conductivity coefficient, gravitational force respectively.

3. Flow Modelling

The equations for the kinetic energy (κ) and specific dissipation rate of kinetic energy (ω) used in the SST $\kappa - \omega$model [12] are given as

$$div\left(\rho_m \kappa \vec{V}_m\right) = div\left\{\left(\mu_m + \frac{\mu_{t,m}}{\sigma_k}\right) grad\ \kappa\right\} + G_\kappa - \rho_m \kappa\omega\, \beta_1 \tag{4}$$

$$div\left(\rho_m \omega \vec{V}_m\right) = div\left\{\left(\mu_m + \frac{\mu_{t,m}}{\sigma_\omega}\right) grad\ \omega\right\} + G_\omega - \rho_m \omega^2 \beta_2 + 2(1 - F_1)\rho_m\, \sigma_{\omega,2}\, \frac{grad\ \omega\ grad\ \kappa}{\omega} \tag{5}$$

In these equations, G_κ represents the generation of turbulence kinetic energy due to the mean velocity gradients, G_ω represents the production ofω, σ_k and σ_ω are the effective Prandtl numbers for the kinetic energy and specific rate of dissipation, respectively; and turbulent viscosity $\mu_{t,m}$ is modelled as

$$\mu_{t,m} = \frac{\rho_m \kappa}{\omega} \frac{1}{max\left(\frac{1}{\alpha^*}, \frac{SF_2}{\alpha_1 \omega}\right)} \tag{6}$$

where $F_1\ and\ F_2$ are the blending functions, S is the strain rate magnitude and α^* is a model constant. Also, the model constants are $\beta_1 = 0.075$, $\beta_2 = 0.0828$, $\alpha_1 = 0.31$, $\sigma_k = 1.0$ and $\sigma_\omega = 1.168$. Further information is available in Fluent [13] for flow modelling.

4. Boundary Conditions

To solve the system of nonlinear partial differential equations, following boundary conditions are used.

At the pipe inlet, a uniform velocity ($v_{x,in}$) as well as a uniform temperature ($T_{in} = 293\ K$) with a turbulent intensity ($I = 2$ to 4%) and hydraulic diameter ($D_h = 0.019\ m$) are stated. And, all the thermal properties used in this work are calculated at the inlet temperature (T_{in}) that also is considered to be the reference temperature.

At the pipe outlet, a static gauge pressure, $p_{gauge} = 0$, is specified. And, the finite volume solver extrapolates the other flow and the scalar quantities such as the temperature and the turbulent quantities from the interior domain.

On the pipe wall, a no-slip boundary condition is introduced with uniform heat flux, q'' = 5000 W/m^2.

5. Entropy Generation

The total entropy generation equation for a circular pipe of length L is proposed by Ratts and Raut [14] and defined as

$$E_{gen} = E_{gen,t} + E_{gen,f} \tag{7}$$

$$E_{gen,f} = \frac{32\dot{m}^3 f L}{\rho_{nf}^2 \pi^2 D_h^5 T_{avg}} \tag{8}$$

$$E_{gen,t} = \frac{\pi D_h^2 \, L \, \dot{q}_s^2}{\lambda_{nf} \, \overline{Nu} \, T_{avg}} \tag{9}$$

where the first term on the right hand side of Eq. (7) is the thermal entropy generation and the second term is the frictional entropy generation where T_{avg} is the average temperature defined as

$$T_{avg} = \frac{(T_{in} - T_{out})}{ln\left(\frac{T_{in}}{T_{out}}\right)} \tag{10}$$

6. Thermophysical Properties

Following relations are considered to calculate the thermophysical properties of Al_2O_3 and TiO_2– water nanofluids

$$\rho_{nf} = (1-\chi)\rho_f + \chi\rho_p \tag{11}$$

$$\left(\rho c_p\right)_{nf} = (1-\chi)\left(\rho c_p\right)_f + \chi\left(\rho c_p\right)_p \tag{12}$$

$$\frac{\lambda_{nf}}{\lambda_f} = 1 + 4.4\, {Re_p}^{0.4} {Pr_f}^{0.66} \left(\frac{T}{T_{fr}}\right)^{10} \left(\frac{\lambda_p}{\lambda_f}\right)^{0.03} \chi^{0.66} \tag{13}$$

$$\frac{\mu_f}{\mu_{nf}} = 1 - 34.87 \left(\frac{d_p}{d_f}\right)^{-0.3} \chi^{1.03} \tag{14}$$

Equations (11) and (12) are considered as classical relationships between the base fluid and nanoparticles, Buongiorno [15]. Equations (13) and (14) are proposed by Corcione [16] with a maximum standard deviation of error of 1.86%.

Here, Re_p is the nanoparticles Reynolds number, defined as

$$Re_p = \frac{\rho_f u_B \, d_p}{\mu_f} = \frac{2\rho_f \kappa_b \, T}{\pi \, {\mu_f}^2 d_p} \tag{15}$$

and d_f is the base fluid molecular diameter defined by

$$d_f = 0.1\left(\frac{6M}{N\pi\rho_f}\right)^{1/3} \tag{16}$$

in which *N* is the Avogadro numberand *M* is the molecular weight of the base fluid.

Also, T_{fr} is the freezing point of the base liquid ($273.16\,K$), κ_b is the Boltzmann constant ($\kappa_b \approx 1.38 \times 10^{-23}\,J/K$), d_p is the diameter of nanoparticles which has a valid range,$10\,nm$ to $150\,nm$ for thermal conductivity and $25\,nm$ to $200\,nm$ for dynamic viscosity of nanofluid, T is the nanofluid temperature, χ is a nanoparticle volume concentration which is valid from0.2% to 9% for thermal conductivity and 0.01 to 7.1% for dynamic viscosity of nanofluids, Pr_f is the Prandtl number of the base fluid. ρ_f,$\left(C_p\right)_f$ and μ_f are the density, heat capacitance and the dynamic viscosity of the base

fluid, respectively, ρ_p and $(C_p)_p$ are the density and heat capacitance of the nanoparticles respectively and u_B is the nanoparticle Brownian velocity which is calculated as the ratio between d_p and the time $\tau_D = {d_p}^2/6D$ by assuming the absence of agglomeration. *D* is the Einstein diffusion coefficient.

The mass density, heat capacitance, kinematic viscosity and thermal conductivity of the base fluid (water) were calculated using the following correlations proposed by Kays and Crawford [17]. All these correlations are valid over $278 \leq T(K) \leq 363$.

$$\rho_f = 330.12 + 5.92\,T - 1.63 \times 10^{-2}T^2 + 1.33 \times 10^{-5}T^3 \tag{17}$$

$$C_{p_f} = 10^{-3} \times (10.01 - 5.14 \times 10^{-2}\,T + 1.49 \times 10^{-4}\,T^2 - 1.43 \times 10^{-7}\,T^3) \tag{18}$$

$$\nu_f = 1.08 \times 10^{-4} - 9.33 \times 10^{-7}\,T + 2.70 \times 10^{-9}\,T^2 - 2.62 \times 10^{-12}T^3 \tag{19}$$

$$\lambda_f = -12.16 + 0.12\,T - 3.66 \times 10^{-4}T^2 + 3.81 \times 10^{-7}T^3 \tag{20}$$

The density, heat capacitance and thermal conductivity of Al_2O_3 at $T = 293\,K$ is considered as Masuda *et al.* [18]:

$$\rho_p = 3880\frac{kg}{m^3},\ C_{p_p} = 773\ \frac{J}{kgK},\ \lambda_p = 36\ \frac{W}{mK}$$

The thermal conductivity of TiO_2 is obtained from the following relation and developed by a curve fitting on the data of Powel *et al.*[19]:

$$\lambda_p = 100 \times (0.1813 - 4.768 \times 10^{-4}\,T + 5.089 \times 10^{-7}T^2), \quad \text{where } 273 \leq T(K) \leq 350 \tag{21}$$

The heat capacitance of TiO_2 is obtained from the following relation and developed by a curve fitting on the data of Smith *et al.*[20]:

$$C_{p_p} = 58.4528 + 3.02195\,T - 3.02923 \times 10^{-3}\,T^2, \quad \text{where } 269.35 \leq T(K) \leq 339.82 \tag{22}$$

The density of TiO_2 is considered as $4250\frac{kg}{m^3}$.

7. Numerical methods and grid sensitivity analysis

The computational domain is formed by using the commercial pre-processor software GAMBIT 2.4.6 which is also used for meshing and setting the boundary conditions. Then the governing non-linear partial differential equations for the continuity, momentum, energy and other scalars, such as, turbulence together with the suitable boundary conditions are discretised. And hence, they are solved by using the Finite volume solver Fluent 6.3.26. The finite volume technique converts the non-linear partial differential equations with the second order upwind scheme to a system of nonlinear algebraic equations that are solved numerically. Second order upwind scheme is employed to achieve higher-order accuracy at the cell faces through a Taylor series expansion of the cell-centred solution about the cell centroid. The pressure-based solver is employed to solve the pressure based equation which is derived from the momentum and continuity equations. All these equations are solved sequentially and

iteratively so as to obtain a converged numerical solution. For all the simulations carried out in the present analysis, convergence criteria for the solutions are considered when the residuals become less than 10^{-6}.

Moreover, extensive computational simulations are performed in order to assess the accuracy of the numerical findings. Initially, the grid sensitivity analysis is performed using both the Standard $k-\omega$ and SST $k-\omega$ transition models to find out an appropriate combination of the mesh distributions. This is applicable to resolve both the velocity and the temperature fields inside the horizontal pipe. The grid sensitivity test is done by varying the total number of grid distributions in both the axial *(Nx)* and the radial *(Nr)* directions. Here, five different grid combinations such as 500×25, 500×50, 500×100, 500×150, and 1000×100 are used. Then, the uniform grid in the axial direction and non-uniform structured grid in the radial direction areconsidered in order to control any large deviations of flow and temperature fields near the upstream as well as near the wall regions. Besides, a mesh successive ratio of 1.1 is considered to generate such non-uniform grids in the near wall region.

Two different test cases are considered for water of Prandtl number, $Pr = 7.04$, $Pr_t = 0.85$ and Reynolds number, Re = 3900 and $10{,}000$ respectively while performing the grid sensitivity test. Then various combinations of grid are analysed to justify that the numerical results are grid independent. Figure 2 shows the variation of radial velocity, temperature (T) and turbulent kinetic energy (κ) profiles at the horizontal location, $x = 0.99$ m, for $K_s = 0$ (smooth pipe wall). These results are generated by using the SST $k-\omega$model and the selection of this particular model for the grid sensitivity test is clarified later. It is observed that the grids 500×100, 500×150 and 1000×100 generate the most reasonable results because the differences found among the results are quite insignificant. In order to save the computing time and to avoid any inconsistencies in the numerical results, particular grid for the present calculations is selected to be consisted of 500 and 100 nodes along the axial and the radial directions respectively.

8. Validation

Validation of the present numerical findings is done for water against the existing experimental data as well as correlations for different $Re = 2300$ to $10^4$and$Pr = 7.04$. Besides, the accuracy of the two different models such as the Standard $\kappa-\omega$ and SST $\kappa-\omega$ models are investigated.In the following, numerical results of Darcy friction factor and Nusselt number are presented and compared with different correlations as well as experimental results. And all the reference data values used in the validation results are also for pure water. Details are given below:

Firstly, numerical results of the Darcy friction factor is compared with the correlation suggested by Blasius [21] and the experimental results of Chandrasekar *et al.* [7] and Naik *et al.* [8]. Then, it is

followed by the comparison of the average Nusselt number with the experimental results of Sharma *et al.* [6], Chandrasekar *et al.* [7] and Naik *et al.* [8] and correlation suggested by Gnielinski [22].

A suitable use of the turbulent intensity at the upstream of the pipe domain is always important for the transient simulation. So, three different values of the turbulent intensity are tested and findings are compared with the relevant data for a smooth pipe wall, as shown in Fig. 3.

The only available correlation for average Nusselt number is the Gnielinski equation [22] which provides a prediction of average Nusselt number for a fully developed turbulent flow in a pipe or channel. This correlation can be useful for a transitional flow because, as suggested, it is valid for $Re > 3000$. However, since it is developed from the data values of a fully developed turbulent flow, its accuracy in transitional flow needs to be tested carefully. The results presented in Fig. 3(b) suggest that this correlation cannot predict the average Nusselt number for the transition flow correctly for all the Reynolds numbers under consideration.

It is observed that Darcy friction factor results of Chandrasekar *et al.* [7] are in good agreement with the results of Blasius [21]. But the Darcy friction factor results of Naik *et al.* [8] found to be slightly lower for low Reynolds numbers and when compared with the results of Blasius [21] and Chandrasekar *et al.* [7]. It is also observed that Nusselt number results of Chandrasekar *et al.* [7] for low Reynolds number seems to be close to the results of Gnielinski [22]. And, Nusselt number results of Sharma *et al.* [6] for high Reynolds number found to be close to the results of Naik *et al.* [8]. Considering these observations, following comparisons are considered:

While varying the turbulent intensity from 2% to 4%, the maximum deviation on the average Nusselt number is found to be 19.45%, 2.94% and 1.85% respectively comparing with the results of Naik *et al.* [8]. On the other hand, the maximum deviation on the Darcy friction factor for I = 2% is 20.49% and 12.68% respectively in comparison with the results of Blasius [21] and Naik *et al.* [8]. And, for the turbulent intensity of 3%, the maximum deviation is 30.93% and 22.39% respectively and is increased further to 35.70% and 26.85% for I = 4%.

Although the turbulent intensity of 2% seems to be a reliable option because of the results of Darcy friction factor showing slightly better agreement with the correlation and experimental results, a significantly higher percentage of deviation in the average Nusselt number is disappointing. A higher Darcy friction factor is observed for the turbulent intensity of 4% compared to that of 3%. And, the maximum percentage deviation between the results of the average Nusselt number for 3% is not significant. That is why, the turbulent intensity of 3% is considered throughout the investigations.

It is also observed that there is no significant variation between the results of average Nusselt number using the Standard $\kappa - \omega$ and the SST $\kappa - \omega$models. But the Darcy friction factor result of the SST $\kappa - \omega$ model is slightly better than that of the Standard $\kappa - \omega$ model in comparison with the

experimental results and correlation. Hence, the SST $\kappa - \omega$ model is considered to carry out all the numerical simulations in this research.

Blasius [21] equation:

$$f = \frac{0.316}{Re^{0.25}}, \qquad 3000 \le Re \le 10^5 \tag{23}$$

Gnielinski [22] equation:

$$\overline{Nu} = \frac{\frac{f}{8}(Re - 1000)\,Pr}{1.0 + 12.7\left(\frac{f}{8}\right)^{0.5}\left(Pr^{\frac{2}{3}} - 1\right)}, \qquad \begin{pmatrix} 0.5 \le Pr \le 2000 \\ 3000 < Re \le 5 \times 10^6 \end{pmatrix}$$
$$f = (1.82 \ln Re - 1.64)^{-2}, \qquad 3000 < Re \le 5 \times 10^6 \tag{24}$$

9. Results and Discussion

Extensive numerical simulations are performed using the single phase model for Al_2O_3-water and TiO_2-water nanofluids with $Re = 2300$ to 10×10^3, $Pr = 7.04$ to 20.29, $\chi = 2$ to 6%, and $d_p =$ 10 to 40 nm. The effects of nanoparticles concentrations and diameters on the heat transfer as well as the entropy generation are discussed in the following sections and some new correlations are also proposed.

9.1 Local and Average Heat Transfer Behaviours

The local and average Nusselt number results are presented and discussed in this section with the purpose of understanding both the local and average heat transfer behaviour. Also, axial variation of the local Nusselt number with different Re ($2000 < Re < 17 \times 10^3$) for the Al_2O_3-water nanofluid ($d_p = 10\,nm, \chi = 2\%$) is shown in Fig. 4. It is observed that the local Nusselt number is always found maximum near the entrance region. Then it starts to decrease rapidly with the axial distance until a minimum value can be predicted from the breakdown of laminar flow. When this minimum value is achieved, Nusselt number starts to increase again and form a plateau-like profile. And finally, it reaches a constant value when the flow tends to be fully developed. Abraham *et al.* [23] also reported the similar behaviour for air flow in pipe under transition flow condition. In addition, the local Nusselt number behaviour is observed to indicate the existence of turbulent flow regime for $Re \ge 17 \times 10^3$.

Moreover, from Fig. 4, it is seen that the distance of laminar breakdown point from the inlet varies from approximately $0.85\,m$ to $0.06\,m$ as the Reynolds number varies from 2300 to 10×10^3. Furthermore, such distance moves to a distance close to the upstream of the pipe when the Reynolds number increases from 2300 to 10×10^3. And then, it tends to decrease rapidly for the Reynolds number that is greater than 10×10^3. In particular, the value of such distance is approximately $0.06\,m$ for $Re = 10 \times 10^3$. However for $Re = 15 \times 10^3$ and 17×10^3, the values of such distance are approximately 0.037 m and 0.0 m respectively. It also means that there is a laminar state between

the upstream and the breakdown point. These outcomes strongly support the observations made by Abraham *et al.* [23] too. It is also observed that the transition behaviour actually begins for $Re > 2000$ and flow becomes fully turbulent for $Re = 17 \times 10^3$. It thus suggests, the transition regime can be extended up to $Re = 17 \times 10^3$ because the distance of break down point from the origin tends to vanish when the Reynolds number is very close to $Re = 17 \times 10^3$. Considering the above observations, we can determine that the transitional regime can be considered as $2000 < Re < 17 \times 10^3$ for the smooth pipe wall case.

Consequently, the following definitions are introduced and the related results are presented in Figs. 5 and 6.

- The distance from the upstream to the laminar breakdown point is called the 'critical distance'.
- Critical distances for flow and thermal fields are known as 'hydrodynamic critical distance' and 'thermal critical distance' respectively.
- Local Nusselt number calculated at the laminar breakdown point is known as critical Nusselt number.

Fig. 5 shows that the hydrodynamic and thermal critical distances decrease along with the increase of Reynolds numbers. It is realistic in a sense that as the Reynolds number increase, flow and thermal transition behaviour tends to diminish and also tends to become fully turbulent. Such behaviour is also physically valid because, in nature, all the flows are turbulent and transition from laminar to turbulent flows will not sustain for a long time. Arithmetically, hydrodynamiccritical distance at $x_{c,V}$ can be calculated from the drops of the velocity gradient on the left and the rises of the velocity gradient on the right. However, thermal critical distance at $x_{c,T}$ can be calculated from the rises of the temperature gradient on the left and the drops of the temperature gradient on the right. It means, the velocity and temperature gradients change sign from the left to the right of the laminar breakdown point. Besides, the hydrodynamic critical distance is also found to be smaller than the thermal critical distance. And, it suggests that transition begins earlier in the flow field than in the temperature field.

As it is also shown in the Fig. 5, the hydrodynamic and thermal critical distances are strongly dependent on the Reynolds number. But, both of them are absolutely independent of different types of fluids, nanoparticles diameters and concentrations. Such findings are realistic and physically valid (Cengel [2]). We find that both the hydrodynamic and thermal entrance lengths are independent of the nanofluids and also of their d_p and χ. While, the hydrodynamic entrance length depends on the Reynolds number and pipe diameter, the thermal entrance length only depends on the pipe diameter. It thus further suggests that when the transition to turbulent flow tends to be fully hydro-dynamically and thermally developed, it remains unaffected by the types of fluids as well as d_p and χ.

In general, significant variations in the flow and temperature fields are observed inside the pipe with the increase of turbulent intensity. Moreover, velocity and temperature critical distances changed significantly with different turbulent intensity. It suggests that both the velocity and temperature critical distances are fully dependent on turbulent intensity.

Finally, two new correlations are proposed to describe the behaviour of hydrodynamic and thermal critical distances with a maximum deviation of 1% under the transition regime. To do this, a total of 80 simulations are carried out for the Reynolds number ranging from 2000 to 17×10^3. These correlations are not valid when $Re \leq 2000$ and $Re > 17 \times 10^3$ because the transition behaviour disappears in this stage. And, fully developed laminar flow ($Re \leq 2000$) and turbulent flow ($Re \geq 17 \times 10^3$) behaviours are observed too.

$$x_{c,V} = Exp\ (A\ log(Re) + B)$$
$$\text{where } A = -1.26306, B = 8.70204, 2000 < Re < 17 \times 10^3 \tag{25}$$

$$x_{c,T} = Exp\ (A\ log(Re) + B)$$
$$\text{where } A = -1.20263, B = 8.27248, 2000 < Re < 17 \times 10^3 \tag{26}$$

Investigations are also carried out for different nanoparticles diameters and concentrations to study their effects on heat transfer and results are presented in the following paragraphs.

Initially, variations of the critical Nusselt number with different Re for $d_p = 10$ to $40\ nm$ and $\chi = 2$ to 6% has are shown in Fig. 6. This figure illustrates that the critical Nusselt number using Al_2O_3-water nanofluid increases with an increase in both the Reynolds number and nanoparticles concentration. Such increase is more significant for the higher value of χ,suggesting that the enhancement of heat transfer rate is strongly dependent on Re and χ. It is also seen that the critical Nusselt number is fully dependent on the type of nanofluids as well as on d_p. This finding is reasonable because the critical Nusselt number has been calculated from the local Nusselt number which also varies with d_p and χ. Similar behaviour also is observed for different d_p of TiO_2-water nanofluid.

The variations of average Nusselt number with the Reynolds number are presented in Fig. 7 considering with the effects of Brownian motion. The purpose is to examine the behaviour of average Nusselt number calculated from the local Nusselt number.

The results presented in Fig. 7 confirm that the average Nusselt number monotonically increases with the increase of nanoparticles concentration. Particularly for Al_2O_3–water nanofluid with $d_p = 10\ nm$, the minimum and maximum percentages of the heat transfer enhancement are approximately 3.25 and 3.40, 11.07 and 11.55, 28.66 and 29.48 respectively. When $d_p = 20\ nm$, such percentages of the heat transfer enhancement are reduced and found approximately 2.27 and 2.36, 7.47 and 7.79, 16.59 and 17.17 respectively. This degeneration of minimum and maximum percentage of heat transfer

continues when d_p increases further. For example, when $d_p = 40\,nm$, they are predicted to be approximately 1.53 and 1.63, 4.71 and 5.11, 10.71 and 11.00 respectively. The trend in which the average *Nu* has changed remains to be the same for the TiO_2–water nanofluid. But, a slight difference in magnitude is obtained for the percentages of the heat transfer enhancement compared to those of the Al_2O_3–water nanofluid.

Overall, the Al_2O_3–water nanofluid always showed the higher heat transfer rate than the TiO_2–water nanofluid irrespective to the change in Reynolds numbers, nanoparticles concentration and diameter when the Brownian motion of nanoparticles is considered. Also, the reason for improving the average Nusselt number is related to different aspects. Increase in the thermal conductivity; Brownian motion of nanoparticles and its size and shape; decrease in the boundary layer thickness and delay in the boundary layer growth are the most prominent ones among them.

Moreover, the percentage of the maximum average heat transfer enhancement predicted by the single phase model is compared with that of the experimental work of Torii [24] and Kim *et al.* [25] in Table 1. Though a different value of the nanoparticle concentration (χ) was used in the experiment, the comparison clearly showed that the model predicting the result is close to that of the experiment [24] with having a maximum deviation of only ~4.33. But the uncertainty of the measurements mentioned in [24] was within a range of 3% which should also need to be accounted while making this comparison. In the other experimental study, Kim *et al.* [25] used the nanoparticle concentration > 1.5 times smaller than the one we simulated for the Al_2O_3-H_2O nanofluid. Thus, a level of variation while comparing between the two sets of result is expected, however when the concentration of the nanoparticle is increased the simulated results showed an incremental rate of the heat transfer. Hence, the percentage rate of the maximum average heat transfers 17. 17 for the Al_2O_3-H_2O nanofluidis predicted to be less than the result of Kim *et al.* [25]. Furthermore, it was reported in the other study by Saha and Paul [10] that a multi-phase model selection may influence the predictive nature of the nanofluid. Consideringfully turbulent flow for which Re > 10000, though the study reported some variation in the heat transfer rate when compared with the single phase model, it was very moderate.

Table 1: Maximum average heat transfer enhancement (%)

References	***Re***	**Nanofluids**	***dp (nm)***	***χ (%)***	**SPM (%)**
Present Work	$2300 \leq Re \leq 10000$	Al_2O_3-H_2O	10	6	29.48
		TiO_2-H_2O			29.34
Present Work	$2300 \leq Re \leq 10000$	Al_2O_3-H_2O	20	6	17.17
		TiO_2-H_2O			17.11
Experimental works					
Torii [24]	$3000 \leq Re \leq 10000$	Al_2O_3-H_2O	10	5	25.01
Kim *et al.* [25]	$3000 \leq Re \leq 6500$	Al_2O_3-H_2O	20	3	20

9.2 Average shear stress ratio analysis

Average shear stress ratio is defined as the ratio of the average shear stresses of nanofluid and water.

In order to understand the behaviour of average shear stress ratio, Figs. 8 show the variation of the nanoparticles concentration and diameter on the average shear stress ratio, $\overline{\tau_\tau}$, with Reynolds number considering the effects of Brownian force of nanoparticles.

When the Brownian motion of nanoparticles is ignored, the average shear stress ratio for the Al_2O_3–water nanofluid with$\chi = 2\%, 4\%$ and 6%, is approximately $1.35, 1.99$ and 3.02 respectively. However, for the TiO_2–water nanofluid the ratio is approximately $1.25, 1.71$ and 2.47 respectively. It suggests, although nanofluids have significant effects on the enhancement of heat transfer, some disadvantages on the wall shear stress is unavoidable. Brownian motion of nanoparticles even causes further drawback, as shown in Fig. 8, resulting in higher values of the average shear stress ratio though depending on d_p. In particular, the average shear stress ratio for Al_2O_3–water nanofluid, is approximately 1.66, 3.58 and 14.60 respectively for χ = 2%, 4% and 6% with $d_p = 10\,nm$. This is reduced to approximately 1.47, 2.54 and 5.79 respectively with $d_p = 20\,nm$ and is further reduced with the higher values of d_p. Additionally, a rapid reduction in the average shear stress ratio is also predicted whenχ is increased and this remains to the case for all the cases investigated. To compare these two nanofluids, the prediction of $\overline{\tau_\tau}$ is almost same apart from the higher value of χ for which some variations in $\overline{\tau_\tau}$ are also reported. Further, the wall shear stress ratio of nanofluids is always found to be higher than that of water and such enhancement is independent to the Reynolds numbers.

Therefore, a significant setback with respect to various practical applications of the nanofluids can be encountered as the effect of the wall shear stress.

9.3 Entropy generation analysis

It is crucial to determine the appropriate nanoparticles concentration as well as the diameter while using nanofluids. For, these are required to calculate the optimal Reynolds numbers. Here, entropy generation analysis suggests a way to work on the issue. The necessary equations used in the entropy generation analysis are given in §5. Besides, when Brownian motion of nanoparticles is considered, the results of the entropy generation analysis are presented in the following paragraphs:

Figure 9 and 10 show the variations of the frictional, thermal and total entropy generations with Reynolds numbers for the two nanofluids. It is seen that the total entropy generation decreases as the Reynolds number increases with the decrease of the nanoparticles diameter from 40 to 10 *nm*. This is caused by the decrease of the thermal entropy generation with the significant enhancement of heat transfer rate already shown in Fig. 7. However, when χ is increased from 2% to 6%, the total entropy generation rapidly decreases as the Reynolds number increases due to the enhancement of average Nusselt number as well as the increase of thermal conductivity of nanofluids. Additionally, the rapid

reduction of total entropy generation indicates that the effect of friction entropy generation is negligible, as shown in Fig. 10. Whereas, the effect of thermal entropy generation is more significant and that is why, the behaviour of both the thermal and total entropy generation is similar.

The total entropy generation also becomes maximum for low Reynolds numbers but with higher χ. While, this finding indicates that an increase in χ has an impact on the total entropy generation being reduced. However, no optimal Reynolds number is observed which could minimise the total entropy generation. It further suggests that suitable χ and d_p which could potentially help to find an optimal thermal system are not found.

9.4 Correlations

Developing a correlation is necessary to determine an average Nusselt number for a particular selection of Reynolds number, nanoparticles concentration as well as diameter. The main advantage here is that one can generate the value of average Nusselt number at any given parameters without running a full set of numerical simulations. Thus it reduces the time, cost and effort required to engineering practice too.

The following correlations are developed for the numerical computation of the average Nusselt number by using a non-linear regression analysis. These correlations are fully dependent on the Reynolds numbers, the Prandtl numbers as well as the d_p. At the same time, these are also valid when the Brownian motion of nanoparticles is taken into account.

The value of maximum standard deviation of error for the Al_2O_3-water nanofluid is found to be 0.21%. Though, it is 0.19% for the TiO_2-water nanofluid. Besides, a validation between the present numerical results of the average Nusselt number and the suggested correlations are presented in Fig. 11. This figure confirms having a good agreement between the numerical results and the proposed correlations.

Single Phase Model (SPM):

Al_2O_3-H_2O nanofluid $: \overline{Nu} = 0.03945\, Re^{0.76746} Pr^{0.24025} \left(\frac{d_f}{d_p}\right)^{-0.0004483}$ (27)

TiO_2-H_2O nanofluid $: \overline{Nu} = 0.03930\, Re^{0.76745} Pr^{0.24165} \left(\frac{d_f}{d_p}\right)^{-0.0007074}$ (28)

where

$$2300 \leq Re \leq 10 \times 10^3, 8.45 \leq Pr \leq 20.29, 10 \leq d_p(nm) \leq 40, 0 < \chi(\%) \leq 6.$$

10. Conclusion

In this research, heat transfer analysis, thermal performance factor and entropy generation analysis have been presented to investigate the effect of smooth pipe wall surface of transition nanofluids flow inside a circular pipe using single phase model. Investigation is carried out for the parameters such as

Reynolds number, nanoparticles concentration, without and with Brownian motion and diameter of nanoparticles. According to our investigations, summary of the overall findings are presented in the following way:

1. It is seen that Al_2O_3-water nanofluid shows slightly higher values of mean velocity and turbulent kinetic energy than TiO_2-water nanofluid.

2. It is also seen that nanoparticles diameter of $d_p \geq 40\,nm$ produces similar results of flow and thermal fields for both the nanofluids.

3. It is found that without and with Brownian motion of nanoparticles and diameters and concentrations of nanoparticles have insignificant effect on Darcy friction factor and that result no penalty in the pumping power.

4. It is also found that Al_2O_3-water nanofluid shows slightly higher heat transfer rate than TiO_2-water nanofluid when without and with Brownian motion of nanoparticles and diameters and concentrations of nanoparticles are considered.

5. It is observed that average wall shear stress ratio of Al_2O_3-water nanofluid is slightly higher than of TiO_2-water nanofluid.

6. No optimal Reynolds number is been observed which can minimize the total entropy generation.

Ethical Statements:

Funding: This study was funded by College of Science and Engineering, University of Glasgow, UK, 2011-15 and Scottish Overseas Research Student Award Scheme (SORSAS), UK, 2011-14.

Conflict of Interest: No conflict of interest.

Nomenclature

A	Acceleration *(m/s^2)*
β_1, β_2, α^*, α_1	Model constants
C_p	Specific heat capacity *(J/kg K)*
D	Einstein diffusion coefficient
D_h	Diameter of a pipe *(m)*
d_f	Fluid molecular diameter *(m)*
d_p	Diameter of nanoparticle *(nm)*
E_{gen}	Entropy generation *(W/K)*
F_1, F_2	Blending functions
F	Darcy friction factor
f_{drag}	Drag function
G_κ	Generation of turbulent kinetic energy
G_ω	Production of ω
H	Enthalpy *(J/kg)*
I	Turbulent intensity
L	Length *(m)*
M	Molecular weight of the base fluid
$\dot{m}$	Mass flow rate *(kg/s)*
N	Avogadro number
N_x, N_r	Number of grid distribution in axial and radial directions
Nu	Nusselt number
P	Pressure *(N/m^2)*
Pr	Prandtl number
$\dot{q}_s$	Heat flux of the pipe *(W/m^2)*
R	Radius of a pipe *(m)*
Re	Reynolds number
R	Radial coordinate *(m)*
S	Modulus of the mean rate of strain tensor
SPM	Single phase model
T	Time average temperature *(K)*
u_B	Nanoparticle particle mean Brownian velocity *(m/s)*
u_τ	Friction velocity *(m/s)*
$\vec{V}$	Time average velocity vector*(m/s)*
x_c	Critical distance*(m)*

Greek symbols

P	Density (kg/m^3)
μ	Dynamic viscosity (kg/ ms)
Λ	Thermal conductivity $(W/m\ K)$
K	Turbulent kinetic energy (m^2/s^2)
Ω	Specific rate of turbulent dissipation (m^2/s^3)
ν	Kinematic viscosity (m^2/s)
σ_t	Constant of turbulent Prandtl number
μ_t	Turbulent molecular viscosity
σ_κ	Effective Prandtl number for turbulent kinetic energy
σ_ω	Effective Prandtl number for specific rate of dissipation
X	Nanoparticles concentration
τ_D	Time (s)
$\overline{\tau_\tau}$	Ratio of average shear stresses

Subscripts

Avg	Average
Eff	Effective
F	Base fluid
Fr	Freezing
In	Inlet
M	Mixture
Mean	Mean
nf	Nanofluid
Out	Outlet
P	Nanoparticles
S	Secondary phase
W	Wall

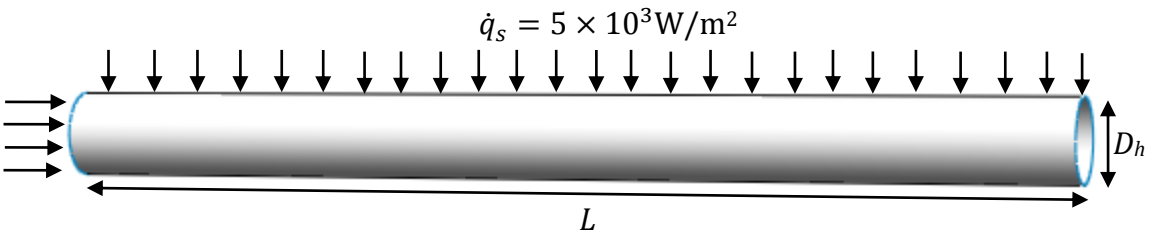

Figure 1: Schematic diagram of the geometry under consideration

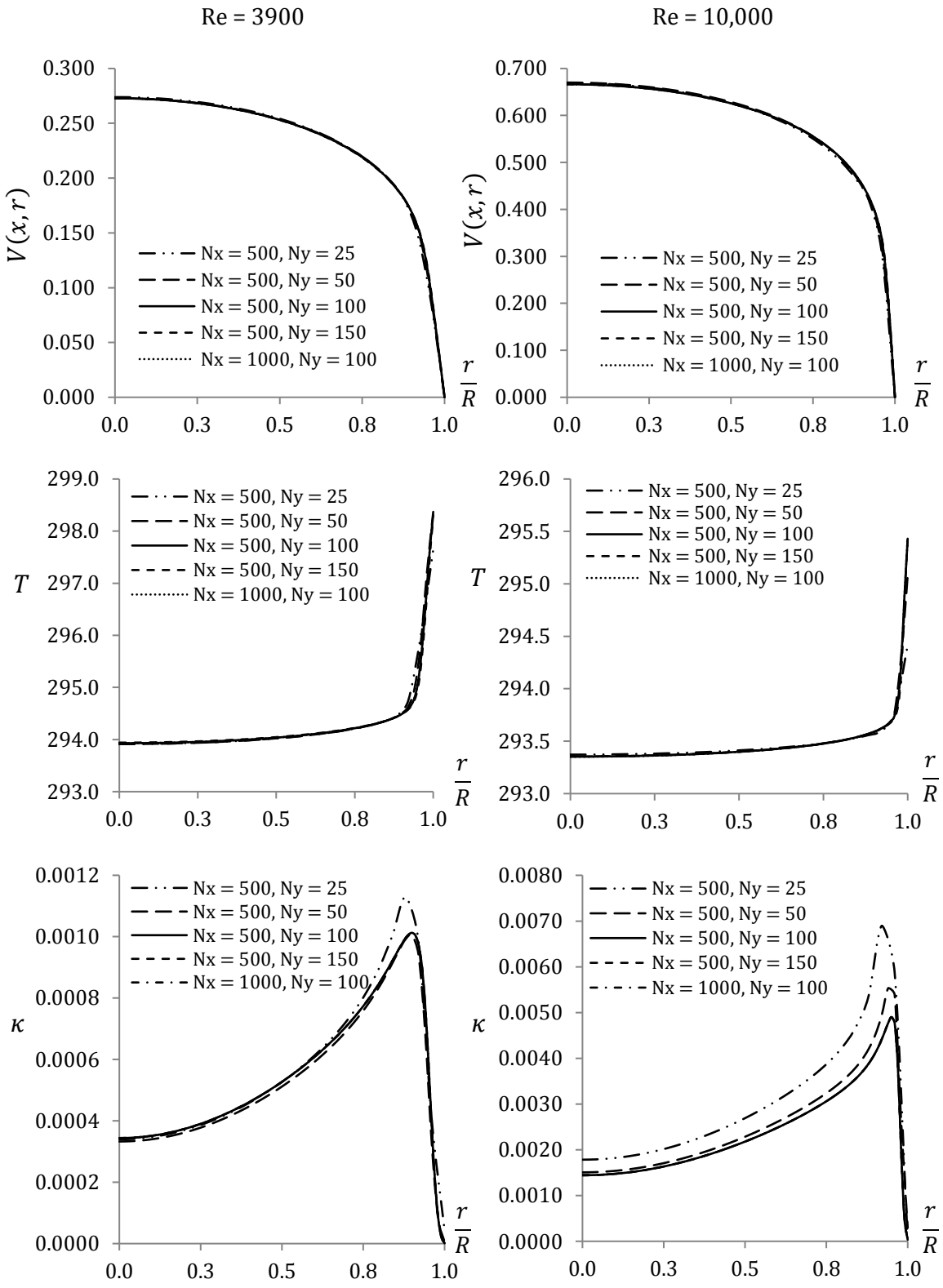

Figure 2: Variations of radial velocity, temperature and turbulent kinetic energy at $x = 0.99\ m$

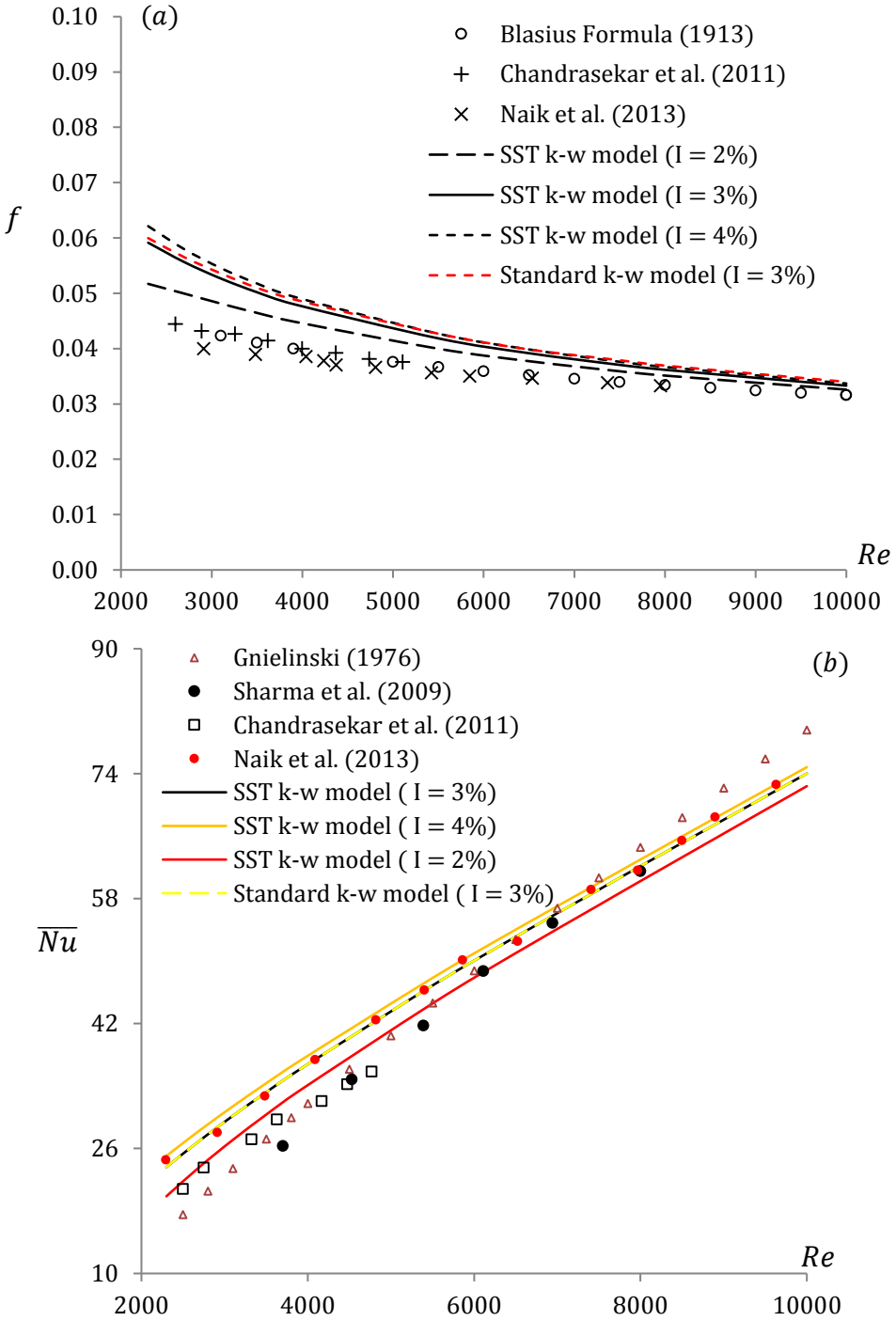

Figure 3: Comparisons of the (a) Darcy friction factor, f and (b) average Nusselt number of water with different correlations and experimental results for different Re

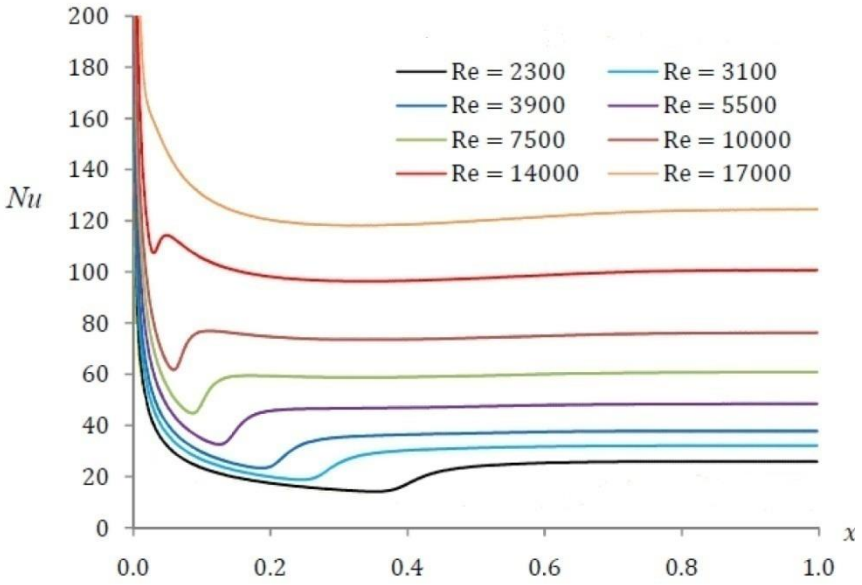

Figure 4: Axial variations of the local Nusselt number with different *Re* for Al_2O_3-H_2O nanofluid, d_p = 10 *nm* and χ = 2% when Brownian motion of nanoparticles is considered

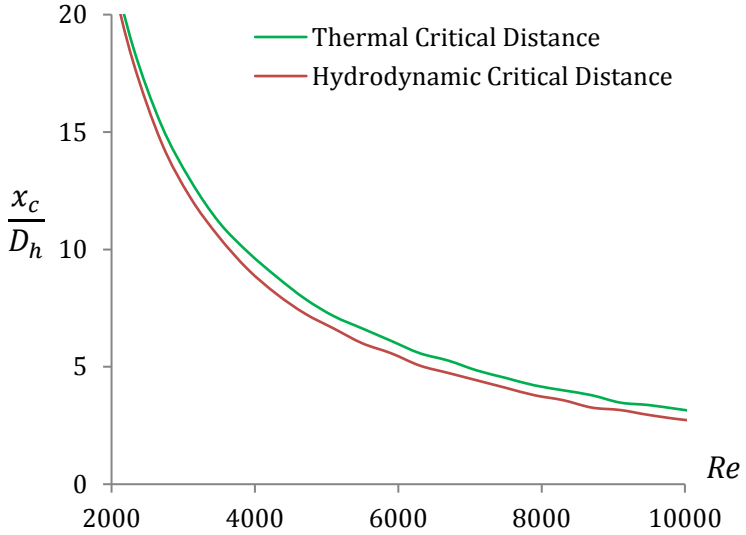

Figure 5: Variations of the hydrodynamic and thermal critical distances with different Reynolds numbers

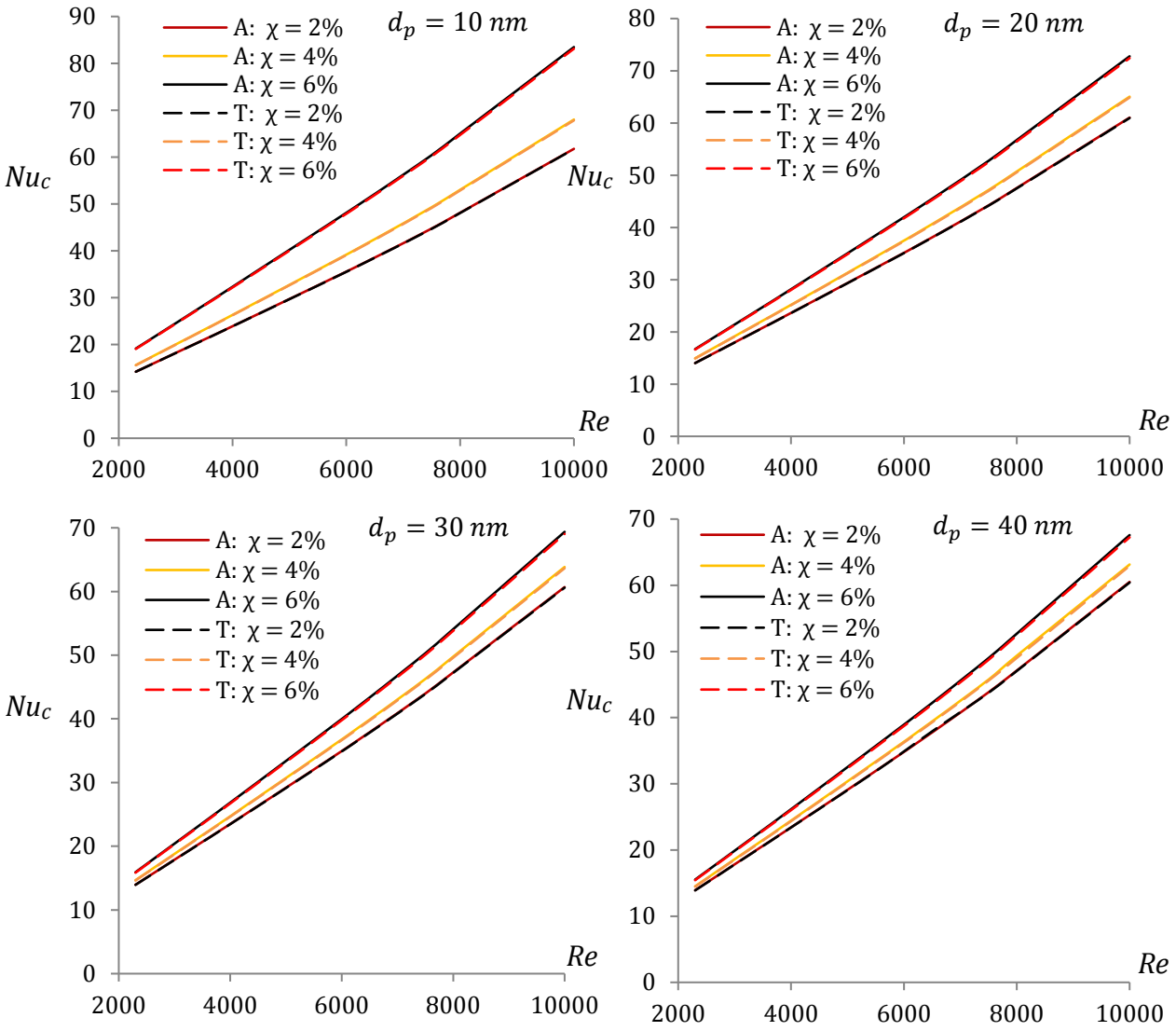

Figure 6: Variations of critical Nusselt number with different Reynolds numbers. (Al_2O_3-water (A) and TiO_2-water (T) nanofluids)

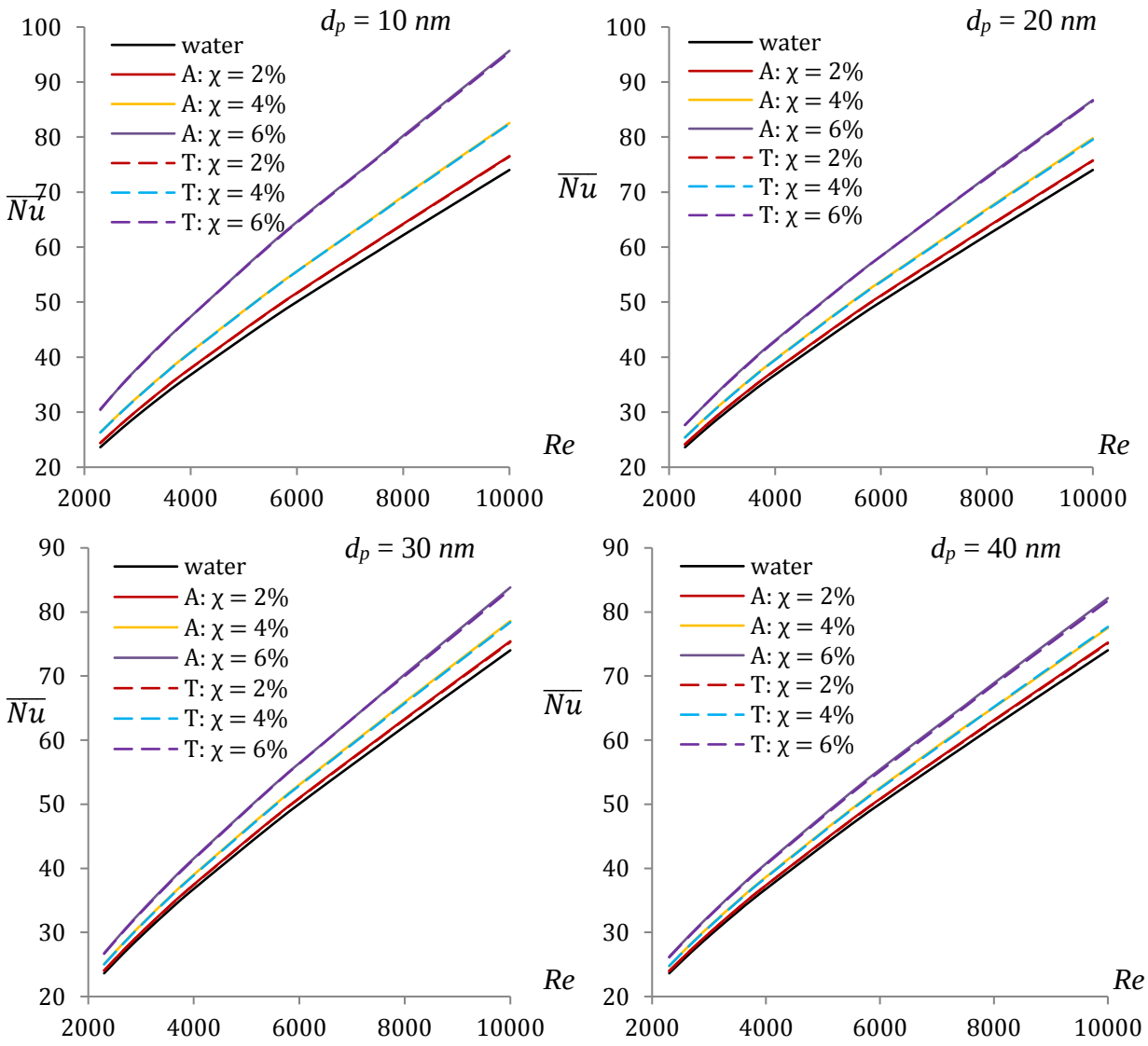

Figure 7: Variations of average Nusselt number with different *Re* and χ for smooth pipe wall case when Brownian motion of nanoparticles is considered

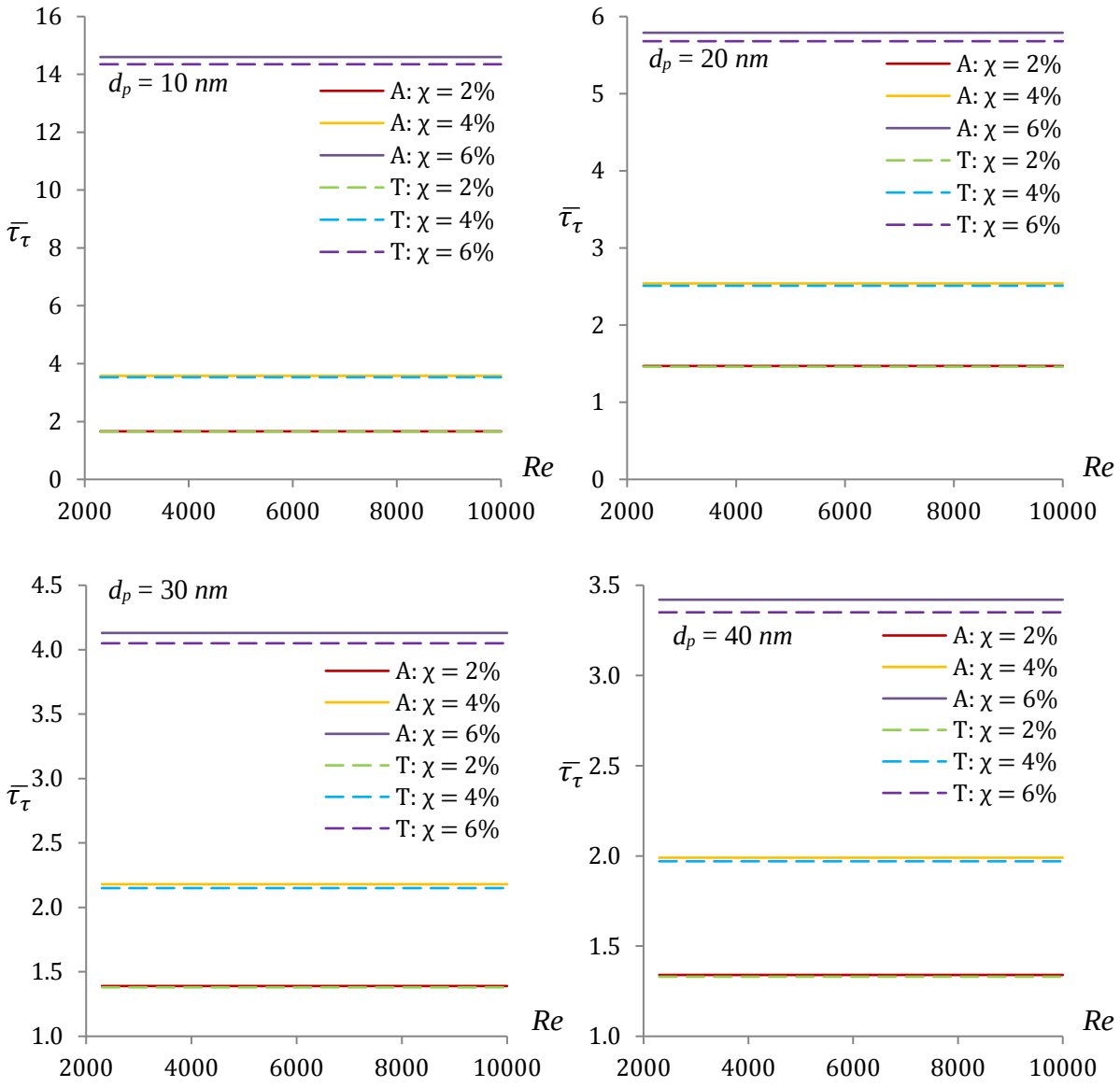

Figure 8: Variations of average shear stress ratio with different *Re* and χ when Brownian motion of nanoparticles is considered

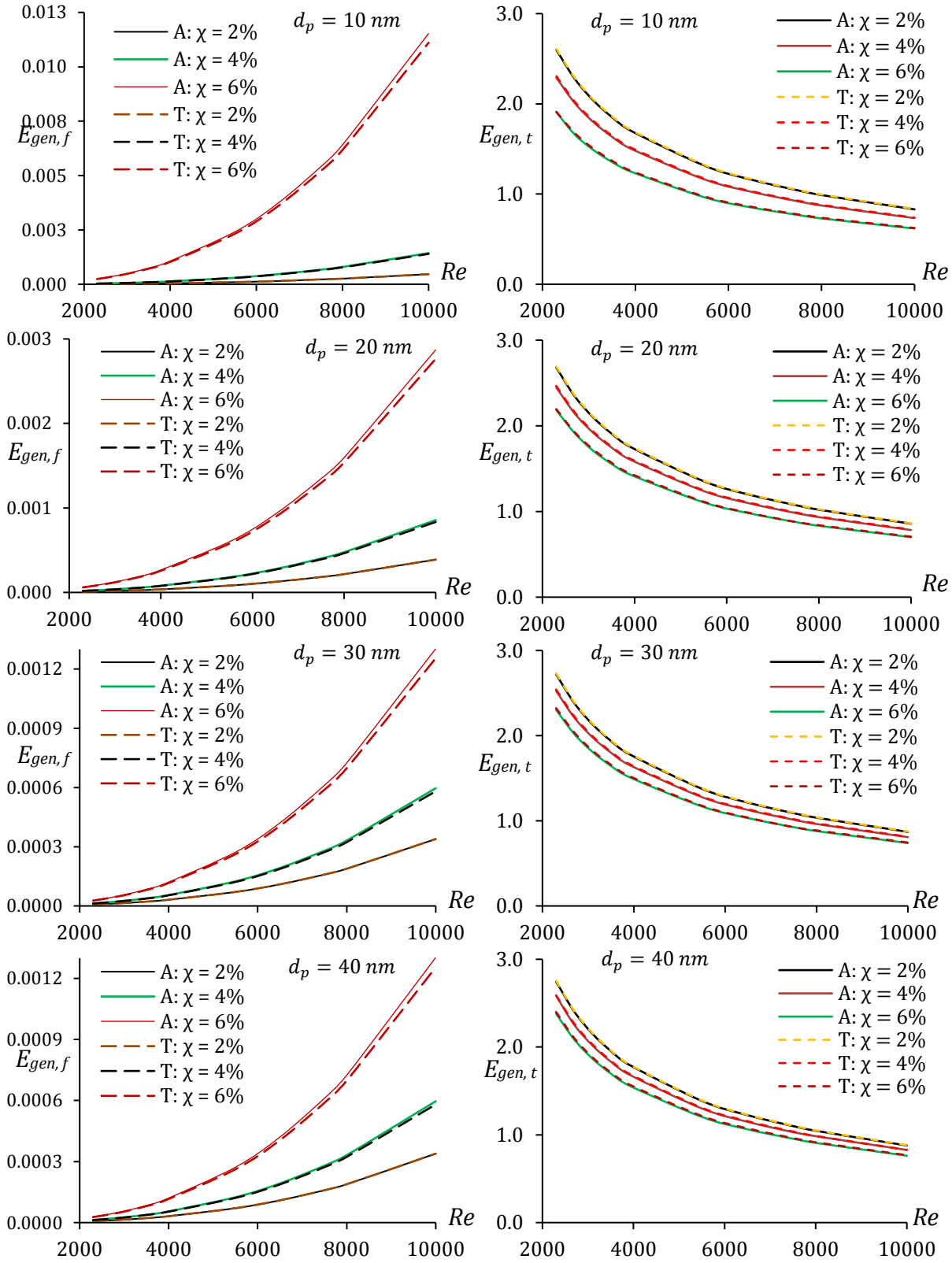

Figure 9: Variations of frictional (left) and thermal entropy generations with different *Re*

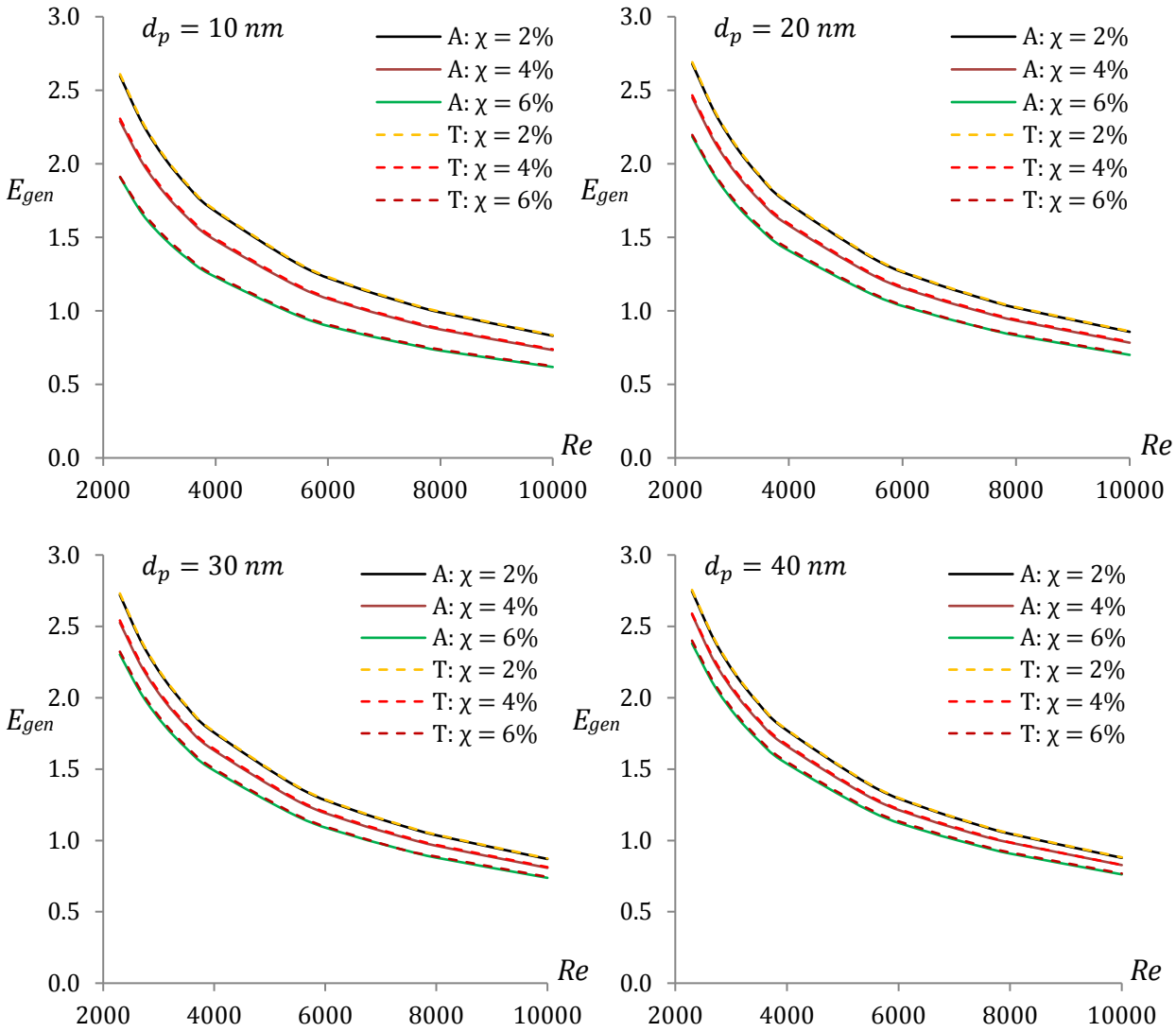

Figure 10: Variations of total entropy generation with different *Re* when Brownian motion of nanoparticles is considered

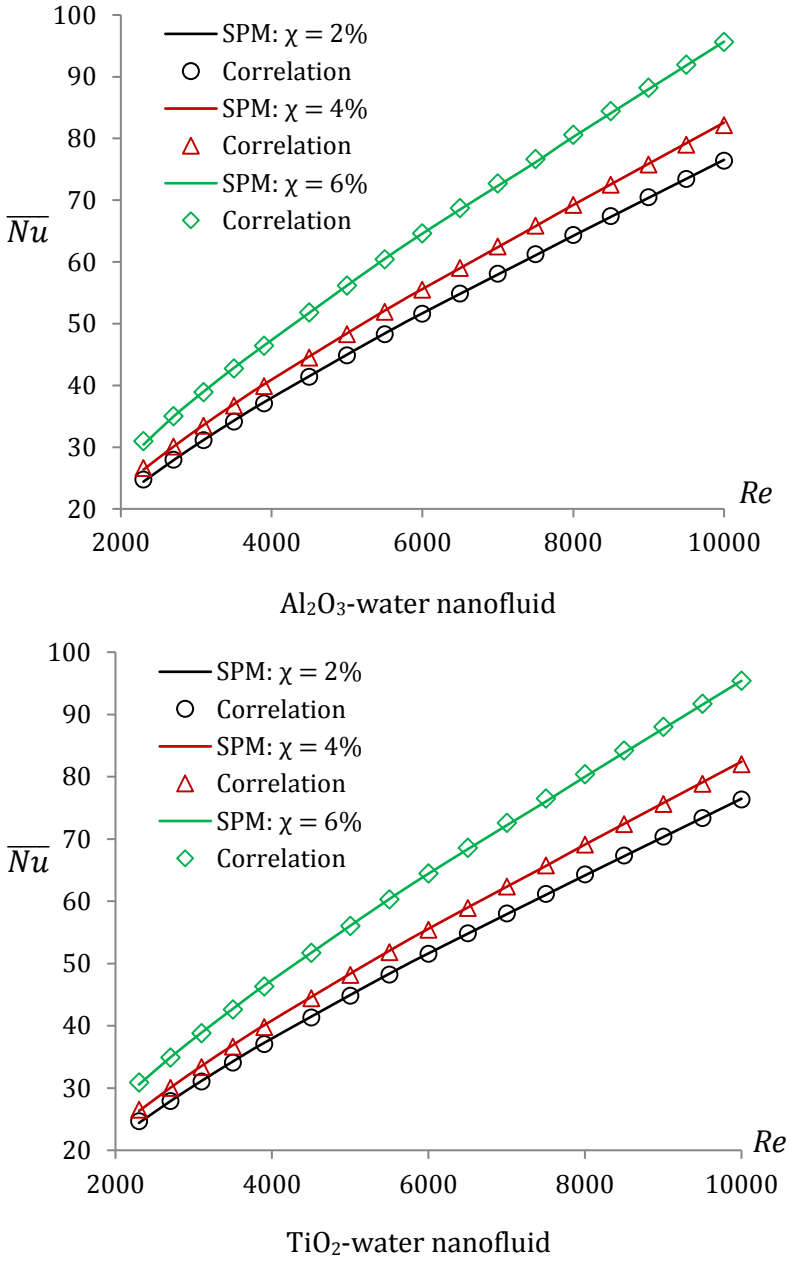

Figure 11: Validations of the proposed correlations with the numerical results of Al_2O_3-water and TiO_2-water nanofluids for d_p = 10 *nm* when Brownian motion of nanoparticles is considered

References

[1] O. Reynolds, An Experimental Investigation of the Circumstances Which Determine Whether the Motion of Water Shall Be Direct or Sinuous, and of the Law of Resistance in Parallel Channels, Philosophical Transactions of the Royal Society of London, 174 (1883) 935-982.

[2] Y.A. Cengel, Heat Transfer: A Practical Approach, 2nd ed., McGraw Hill, New York, 2003.

[3] V.W. Ekman, On the change from steady to turbulent motion of liquids, Ark. f. Mat. Astron. och Fys., 6 (1910).

[4] W. Pfenniger, Boundary Layer and Flow Control, LACHMAN, G. V. ed., Pergamon, 1961.

[5] C.C. Tang, S. Tiwari, M.W. Cox, Viscosity and Friction Factor of Aluminum Oxide–Water Nanofluid Flow in Circular Tubes, Journal of Nanotechnology in Engineering and Medicine, 4 (2013) 1-6.

[6] K.V. Sharma, L.S. Sundar, P.K. Sarma, Estimation of heat transfer coefficient and friction factor in the transition flow with low volume concentration of Al_2O_3 nanofluid flowing in a circular tube and with twisted tape insert, International Communications in Heat and Mass Transfer, 36 (2009) 503-507.

[7] M. Chandrasekar, S. Suresh, A.C. Bose, Experimental studies on heat transfer and friction factor characteristics of Al_2O_3/water nanofluid in a circular pipe under transition flow with wire coil inserts Heat Transfer Engineering, 32 (2011) 485-496.

[8] M.T. Naik, G.R. Janardana, L.S. Sundar, Experimental investigation of heat transfer and friction factor with water–propylene glycol based CuO nanofluid in a tube with twisted tape inserts, International Communications in Heat and Mass Transfer, 46 (2013) 13-21.

[9] J.P. Meyer, T.J. McKrell, K. Grote, The influence of multi-walled carbon nanotubes on single-phase heat transfer and pressure drop characteristics in the transitional flow regime of smooth tubes, International Journal of Heat and Mass Transfer, 58 (2013) 597–609.

[10] G. Saha, M.C. Paul, Numerical analysis of heat transfer behaviour of water based Al_2O_3 and TiO_2 nanofluids in a circular pipe under the turbulent flow condition, International Communications in Heat and Mass Transfer, 56 (2014) 96-108.

[11] G. Saha, M.C. Paul, Heat transfer and entropy generation of turbulent forced convection flow of nanofluids in a heated pipe, International Communications in Heat and Mass Transfer, 61 (2015) 26-36.

[12] F.R. Menter, Two-equation eddy-viscosity turbulence models for engineering applications, AIAA Journal, 32 (1994) 1598-1605.

[13] Fluent 6.3 user guide, Fluent Inc., Lebanon, 2006.

[14] E.B. Ratts, A.G. Raut, Entropy generation minimization of fully developed internal flow with constant heat flux, Journal of Heat Transfer, 126 (2004) 656-659.

[15] J. Buongiorno, Convective transport in nanofluids, Journal of Heat Transfer, 128 (2006) 240-250.

[16] M. Corcione, Empirical correlating equations for predicting the effective thermal conductivity and dynamic viscosity of nanofluids, Energy Conversion and Management, 52 (2011) 789-793.

[17] W.M. Kays, M.E. Crawford, Convection heat and mass transfer, 2nd ed., McGraw Hill, New York, 1980.

[18] H. Masuda, A. Ebata, K. Teramae, N. Hishinuma, Alternation of thermal conductivity and viscosity of liquid by dispersing ultra-fine particles (dispersion of Al_2O_3, SiO_2 and TiO_2 ultra-fine particles), Netsu Bussei, 40 (1993) 227-233

[19] R.W. Powell, C.Y. Ho, P.E. Liley, Thermal conductivity of selected materials, United states department of commerce, National Bureau of standards, 1962.

[20] S.J. Smith, R. Stevens, S. Liu, G. Li, A. Navrotsky, J.B. Goates, B.F. Woodfield, Heat capacities and thermodynamic functions of TiO_2 anatase and rutile: analysis of phase stability, Am. Mineral, 94 (2009) 236-243.

[21] H. Blasius, Grenzschichten in Flussigkeiten mit kleiner reibung (German), Z. Math. Physics 56 (1908) 1-37.

[22] V. Gnielinski, New equations for heat and mass transfer in turbulent pipe and channel flow, International Chemical Engineering, 16 (1976) 359-368.

[23] J.P. Abraham, E.M. Sparrow, J.C.K. Tong, Heat transfer in all pipe flow regimes: laminar, transitional/intermittent, and turbulent, International Journal of Heat and Mass Transfer, 52 (2009) 557-563.

[24] S. Torii, Turbulent heat transfer behavior of nanofluid in a circular tube heated under constant heat flux, Advances in Mechanical Engineering, (2010) 917612: 1-7.

[25] D. Kim, Y. Kwon, Y. Cho, C. Li, S. Cheong, Y. Hwang, J. Lee, D. Hong, S. Moon, Convective heat transfer characteristics of nanofluids under laminar and turbulent flow conditions, Current Applied Physics, 9 (2009) 119-123.